



# Ca isotopes record rapid crystal growth in volcanic and subvolcanic systems

Michael A. Antonelli<sup>a,1,2</sup>, Tushar Mittal<sup>a</sup>, Anders McCarthy<sup>b</sup>, Barbara Tripoli<sup>a</sup>, James M. Watkins<sup>c</sup>, and Donald J. DePaolo<sup>a</sup>

<sup>a</sup>Department of Earth and Planetary Science, University of California, Berkeley, CA 94720; <sup>b</sup>School of Earth Sciences, University of Bristol, BS8-1RL Bristol, United Kingdom; and <sup>c</sup>Department of Earth Sciences, University of Oregon, Eugene, OR 97403

Edited by Mark H. Thiemens, University of California San Diego, La Jolla, CA, and approved September 5, 2019 (received for review May 23, 2019)

Kinetic calcium isotope effects can be used as growth-rate proxies for volcanic and subvolcanic minerals. Here, we analyze Ca isotopic compositions in experimental and natural samples and confirm that large kinetic effects ( $>2\text{\textperthousand}$ ) can occur during magmatic plagioclase crystallization. Experiments confirm theoretical predictions that disequilibrium isotope effects depend mainly on the rates for crystal growth relative to liquid phase Ca diffusivity ( $R/D$ ). Plagioclase phenocrysts from the 1915 Mount Lassen rhodacite eruption, the ~650-y-old Deadman Creek Dome eruption, and several mafic subvolcanic orbicules and plagioclase comb layers from Northern California have disequilibrium Ca isotopic compositions that suggest rapid crystal growth rates ( $>1 \text{ cm/y}$  to  $15 \text{ cm/y}$ ). The Ca isotope results, combined with complementary crystal-size distribution analyses, suggest that magmatic rejuvenation (and eruption) events, as reflected in crystal growth times, can be as short as  $\sim 10^{-3} \text{ y}$ . Although mafic systems are predicted to have shorter magmatic rejuvenation periods, we find similarly short timescales in both mafic and silicic systems. These results are consistent with a growing body of evidence suggesting that dominantly crystalline volcanic magma reservoirs can be rapidly reactivated by the injection of fresh magma prior to eruption. By focusing on a common mineral such as plagioclase, this approach can be applied across all major magmatic compositions, suggesting that Ca isotopes can be used as a tool for investigating the dynamics and timing of volcanic eruptions.

Ca isotopes | volcanic eruptions | magma recharge | crystal growth | timescales

The processes and timescales of magmatic rejuvenation and eruption events are important to understand because of their bearing on modern volcanic hazards and on Earth's climate over geologic time (1). Although our understanding of volcanic processes has greatly improved in the last several decades, it is still difficult to test associated physical models for magmatic recharge and eruption (e.g., refs. 2–5). Recent progress has been made in estimating magmatic rejuvenation timescales in volcanic systems, which are often found to be several orders of magnitude shorter than the residence times determined from absolute ages of crystals in the erupted magma (e.g., refs. 6–10). These timescale constraints enable us to directly test various geophysical hypotheses and to better interpret signals during modern volcanic unrest (e.g., changes in shallow seismicity, seismic wave speeds, and fumarole/gas emissions). The short growth timescales relative to crystal residence times suggest that volcanic magma chambers are kept in a largely crystalline immobile state for a majority of their lifetimes (“cold storage”) and are episodically reactivated by injection of fresh (hot) magma into the system (magmatic recharge/rejuvenation) shortly before eruption (2–4, 11–16).

To determine these preeruption timescales, 3 sets of tools are commonly used: 1) U-Pb dating, 2) elemental diffusion profiles in minerals, and 3) crystal-size distribution (CSD) analyses (7). Each of these methods is applicable only to some systems, and each can be potentially biased. Diffusion profiles and CSD analyses, for example, must necessarily assume crystal growth rates in order to

get at relevant timescales (7), which may be especially inaccurate for rapid crystallization of phenocryst populations directly prior to a volcanic eruption. Similarly, U-Pb dating of zircons is biased toward silicic magmas and absolute crystal residence times, while Fe and Mg diffusion profiles (e.g., in olivine) can only be used in mafic systems. These methodological biases, based on the bulk compositions of the magma, may lead to systematic differences in results for mafic and silicic volcanism, where mafic systems are inferred to have shorter rejuvenation timescales (7). Here, we use an approach for measuring crystal growth rates, based on kinetic Ca isotope fractionations that accompany rapid crystallization of plagioclase in volcanic systems. We demonstrate that these growth rates can then be used to constrain crystallization timescales by either focusing on phases that are likely to form shortly prior to (or during) volcanic eruptions (magmatic orbicules and plagioclase comb layers) or by combining phenocryst growth-rate estimates with CSD analyses.

## Samples

We analyze Ca isotope abundances by thermal ionization mass spectrometry (TIMS), where the resultant measured parameter is denoted as  $\delta^{44}\text{Ca}$  (expressed in per mil and defined as  $10^3[(^{44}\text{Ca}/^{40}\text{Ca})_{\text{sample}}/(^{44}\text{Ca}/^{40}\text{Ca})_{\text{BSE}} - 1]$ ), in plagioclase phenocrysts and glass separates from 3 rapidly cooled experimental tonalites ( $n = 6$ ), various natural volcanic phenocrysts ( $n = 12$ )

## Significance

Timescale estimates for crystal growth in volcanic systems, which are generally much shorter than absolute crystal ages, are thought to be shortest in mafic (vs. silicic) systems. However, this result may be influenced by assumptions for growth rates and/or methodological biases. We show that Ca isotopes can be used to constrain crystal growth rates in volcanic systems and confirm that large kinetic isotope effects can arise during plagioclase crystallization in natural phenocrystic, orbicular, and experimental samples. Combined with crystal-size distribution analyses, our approach can constrain timescales for phenocryst formation across all major bulk magma compositions, without having to assume crystal growth rates. Our results yield comparable rejuvenation timescales for the silicic and mafic systems studied.

Author contributions: M.A.A. and D.J.D. designed research; M.A.A. and T.M. performed research; T.M., A.M., B.T., and J.M.W. contributed new reagents/analytic tools; M.A.A., T.M., A.M., B.T., J.M.W., and D.J.D. analyzed data; and M.A.A. wrote the paper.

The authors declare no competing interest.

This article is a PNAS Direct Submission.

Published under the PNAS license.

<sup>1</sup>To whom correspondence may be addressed. Email: mantonelli@berkeley.edu.

<sup>2</sup>Present address: Cosmochimie, Astrophysique, et Géophysique Experimentale (CAGE), Institut de Physique du Globe de Paris (IPGP), 75005 Paris, France.

This article contains supporting information online at [www.pnas.org/lookup/suppl/doi:10.1073/pnas.1908921116/-DCSupplemental](http://www.pnas.org/lookup/suppl/doi:10.1073/pnas.1908921116/-DCSupplemental).

and their host matrices ( $n = 6$ ), and mineral separates from a slowly crystallized cumulate gabbro sample ( $n = 3$ , Stillwater Complex, MT; see *SI Appendix* for sample details and *SI Appendix*, Table S1 for chemical compositions). We also analyze  $\delta^{44}\text{Ca}$  in plagioclase separates from magmatic orbicules and comb layers ( $n = 23$ ), and in small whole-rock subsections extracted across the layers of 2 magmatic orbicules ( $n = 26$ ; *SI Appendix*, Figs. S2–S5; chemical compositions in *SI Appendix*, Tables S2 and S3). The layered textures in these latter samples, thought to result from fast crystallization on wall rocks and xenoliths in rapidly decompressing magmas within subvolcanic conduits (17–19), are directly linked to magmatic recharge events and are targeted here to provide additional insight into magmatic timescales from a subvolcanic perspective.

### Kinetic Ca Isotope Fractionation during Crystal Growth

Potential deviations from isotopic equilibrium during rapid crystal growth were first proposed by ref. 20, who developed a model relating isotopic effects to growth rate. Predicted isotopic fractionation effects in this model are based on Ca diffusion through chemically depleted boundary layers around growing crystals, where  $^{40}\text{Ca}$  diffuses faster than  $^{44}\text{Ca}$  (Fig. 1), and depends on 1) crystal growth rates relative to Ca diffusivity ( $R/D$ ), 2) isotopic differences in Ca diffusion coefficients ( $D_{44}/D_{40}$ ), 3) mineral-melt Ca distribution coefficients, and 4) boundary layer thicknesses around the growing crystals (20). Given the development of a steady-state boundary layer during crystal growth (*SI Appendix*), the  $\delta^{44}\text{Ca}$  fractionation between crystals and melt ( $\Delta^{44}\text{Ca}$ ) is given by

$$\Delta^{44}\text{Ca} = 10^3 \left( 1 - \frac{D_{40}}{D_{44}} \right) \frac{R \times \text{BL}}{D_{40}} (1 - K), \quad [1]$$

where  $D_{40}$  and  $D_{44}$  are the diffusivities of  $^{40}\text{Ca}$  and  $^{44}\text{Ca}$  in the melt, respectively,  $R$  is the crystal growth rate, BL is the boundary layer thickness, and  $K$  is the Ca distribution coefficient in the mineral vs. the melt (generally  $K > 1$  in plagioclase). Thicker BLs, higher distribution coefficients, lower Ca diffusivities, and larger differences in isotope-specific diffusivities ( $D_{44}/D_{40}$ ) lead to lower growth-rate estimates for a given  $\Delta^{44}\text{Ca}$ .

We confirm that kinetic isotope fractionations occur during plagioclase phenocryst growth by analyzing samples from rapidly cooled experimental tonalites. Plagioclase and glass were separated from 3 simplified tonalite crystallization experiments (NCASH system [ $\text{Na}_2\text{O}$ ,  $\text{CaO}$ ,  $\text{Al}_2\text{O}_3$ ,  $\text{SiO}_2$ , and  $\text{H}_2\text{O}$ ]) performed at ETH-Zurich (21). The 3 samples have the same initial chemical/isotopic compositions, heating, and cooling trajectories, but contain

variable amounts of dissolved water (1, 1.5, and 2 wt%; *SI Appendix*). Starting materials were held at 1,200 °C and 200 MPa for 24 h and then cooled isobarically to 650 °C in ~10 min, resulting in rapid plagioclase crystallization (*SI Appendix*).

In all experiments, we find that the plagioclase phenocrysts have lower  $\delta^{44}\text{Ca}$  than glass, with  $\Delta^{44}\text{Ca}_{\text{plag-mtx}}$  (defined as  $\delta^{44}\text{Ca}_{\text{plag}} - \delta^{44}\text{Ca}_{\text{mtx}}$ ) lower than  $-2\text{\textperthousand}$  in the experiment with the least  $\text{H}_2\text{O}$  (sample 3-10, shown in Fig. 2A and B). The magnitude of the isotopic fractionations, which are much larger than predicted for minerals at equilibrium (22–24), along with previous multicollector inductively coupled plasma (ICP) mass spectrometry work measuring kinetic slopes for Ca fractionation in triple-isotope space ( $^{42}\text{Ca}/^{44}\text{Ca}$  vs.  $^{48}\text{Ca}/^{44}\text{Ca}$ ) for sample 3-10 (1 wt%  $\text{H}_2\text{O}$ ) (22), rules out the possibility that these are equilibrium partitioning effects. In agreement with previous predictions for increasing Ca diffusivities at fixed growth rates (20), we find that increasing amounts of water in our experiments lead to smaller  $\Delta^{44}\text{Ca}_{\text{plag-mtx}}$  (Fig. 2A and B). The smaller isotopic fractionation is consistent with an order of magnitude increase in Ca diffusivity (for ~1 wt% increase in  $\text{H}_2\text{O}$ ) and does not require changes in isotopic diffusivity ratios ( $D_{44}/D_{40}$ ), in accordance with recent work on Li isotope diffusion in hydrous magmas (25) (*SI Appendix*). These results suggest that kinetic Ca isotope effects are sensitive to the  $R/D$  ratio in volcanic systems.

### Kinetic Ca Isotope Fractionations in Volcanic and Subvolcanic Samples

We measured volcanic phenocrysts from 6 basaltic to rhyolitic samples ( $\delta^{44}\text{Ca}$  ranging from  $-0.4$  to  $+0.2\text{\textperthousand}$ ; Fig. 2C and *SI Appendix*, Fig. S1 and Table S4). Plagioclase has lower  $\delta^{44}\text{Ca}$  than host matrix for all bulk compositions, with  $\Delta^{44}\text{Ca}_{\text{plag-mtx}}$  ranging from  $\sim 0.0$  to  $-0.2\text{\textperthousand}$ , (Fig. 2D). Comparing these samples to plagioclase from the Stillwater cumulate gabbro, which crystallized much more slowly [~10 Ky to 100 Ky (26)] and has previously analyzed equilibrium triple Ca isotope compositions (see figure 6 in ref. 22), we find that it is isotopically heavier ( $\delta^{44}\text{Ca}_{\text{plag}} \approx -0.2\text{\textperthousand}$ ) than volcanic plagioclase, despite having approximately the same bulk rock  $\delta^{44}\text{Ca}$  (Fig. 2C). Clinopyroxene and orthopyroxene separates from this cumulate sample have  $\delta^{44}\text{Ca}$  of  $-0.15\text{\textperthousand}$  and  $+0.5\text{\textperthousand}$ , respectively, in agreement with equilibrium predictions at  $\sim 800$  °C to 900 °C (22, 23, 27, 28). The mafic phenocrysts (clinopyroxene, hornblende, and olivine) have higher  $\delta^{44}\text{Ca}$  than plagioclase and matrix in all samples ( $\Delta^{44}\text{Ca}_{\text{min-mtx}}$  from  $\sim 0.0$  to  $+0.3\text{\textperthousand}$ , Fig. 2 C and D) as generally predicted by ab initio estimates. These differences are in the right direction to be equilibrium effects, but the  $\Delta^{44}\text{Ca}_{\text{min-plag}}$  values suggest that

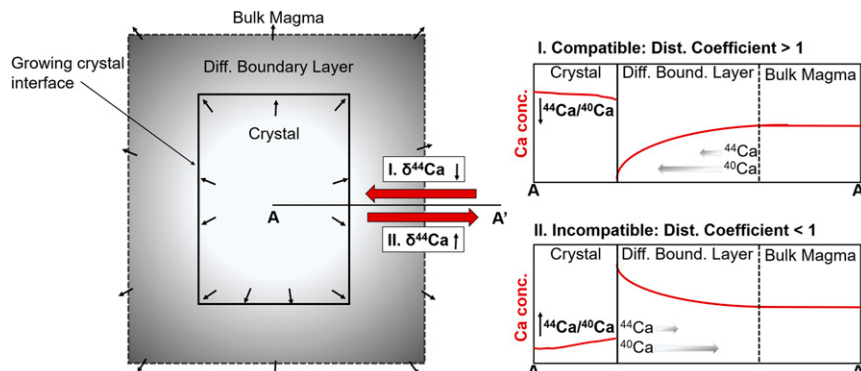


**Fig. 1.** Conceptual diagram for disequilibrium Ca isotope fractionation during rapid crystal growth, as described in ref. 20. The kinetic effects are the result of isotopic rate differences for Ca diffusion through a chemically distinct boundary layer developed around growing crystals (Left). For minerals where Ca is compatible (e.g., plagioclase, clinopyroxene, and amphibole), faster growth leads to increasingly negative deviations from isotopic equilibrium (Top Right), whereas the opposite is true for minerals where Ca is strongly incompatible (e.g., olivine; Bottom Right). diff. boundary layer, diffusive boundary layer; dist. coefficient, distribution coefficient.

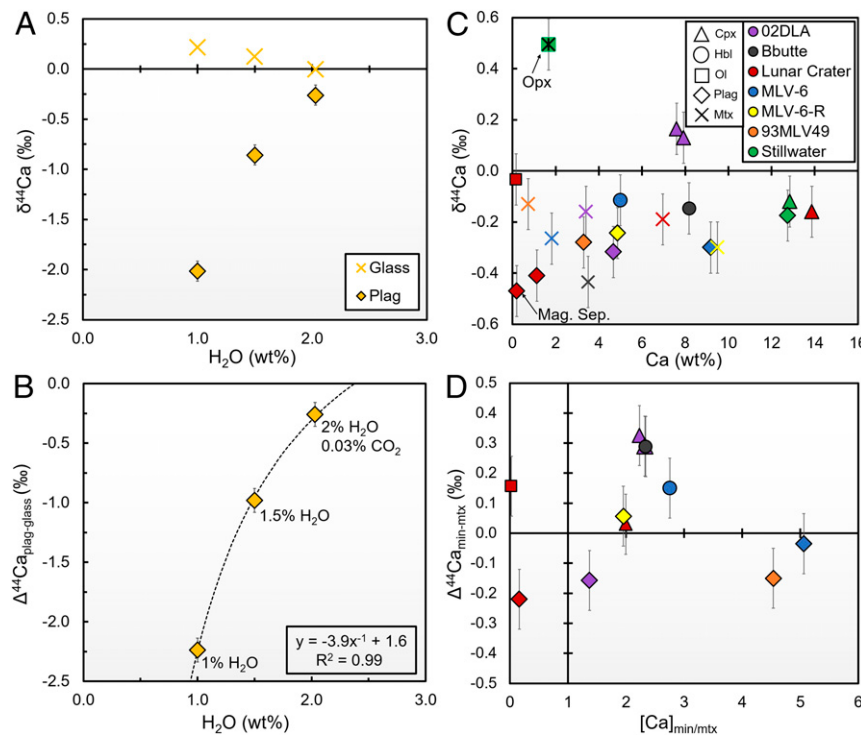


**Fig. 2.** Ca isotope compositions in (A and B) experimental and (C and D) natural phenocrysts and cumulate samples. (A and B) Water concentrations versus (A)  $\delta^{44}\text{Ca}$  in glass and plagioclase (Plag) phenocrysts ( $n = 6$ ) and (B)  $\Delta^{44}\text{Ca}_{\text{plag-glass}}$  ( $n = 3$ ). (C) The  $\delta^{44}\text{Ca}$  in matrix and various mineral separates versus Ca concentrations ( $n = 21$ ). Cpx, clinopyroxene; Hbl, hornblende; Ol, olivine; Plag, plagioclase; Mtx, matrix; Opx, orthopyroxene. (D) Ca isotopic differences between minerals and matrix ( $\Delta^{44}\text{Ca}_{\text{min-mtx}}$ ) versus measured Ca distribution coefficients ( $[\text{Ca}]_{\text{min-mtx}}$ ,  $n = 11$ ). Mafic phenocrysts are isotopically heavier than the melt, whereas plagioclase is isotopically lighter. In C, a rough magnetite separation from Lunar Crater basalt ("mag. sep.") is likely to be contaminated by plagioclase (SI Appendix). Ca isotopic measurements are reported relative to bulk silicate Earth (+0.96‰ relative to SRM915a). Error bars represent long-term 2 SD uncertainties on  $\delta^{44}\text{Ca}$  ( $\pm 0.1\text{\textperthousand}$ ).

there may also be small disequilibrium effects (SI Appendix, Table S4). The observation that clinopyroxene and hornblende (which generally have Ca distribution coefficients of  $>1$ ) are always heavier than matrix, however, suggests that kinetic effects during their crystallization are relatively small compared to those for plagioclase (SI Appendix).

We argue that the observed isotopic fractionations in our natural samples, although small ( $\leq -0.2\text{\textperthousand}$ ), are likely to be nonequilibrium effects that are indicative of crystal growth rate. Although no estimates are currently available for equilibrium mineral-melt Ca isotope partitioning from ab initio or experimental methods, equilibrium Ca isotope fractionation between minerals and melt has been estimated from natural samples (24), where plagioclase is suggested to have negligible mineral-melt fractionations ( $<0.1\text{\textperthousand}$ ). This implies that the  $\Delta^{44}\text{Ca}_{\text{plag-mtx}}$  variations we observe in some of our volcanic samples are more likely to be the result of kinetic effects during phenocryst growth.

In the plagioclase separated from orbicules, comb layers, and associated rocks ( $n = 23$ ; SI Appendix), it is easier to evaluate the kinetic origin of Ca isotope fractionation because each layer is mineralogically similar and comes from the same bulk magma composition (17, 18, 29). Thus we can assume that the differences in plagioclase Ca isotope compositions are due to differences in crystal growth rates. We find a relatively large  $\delta^{44}\text{Ca}_{\text{plag}}$  range (from  $-0.1$  to  $-0.5\text{\textperthousand}$ ), with plagioclase from comb layers and orbicule rims having lower  $\delta^{44}\text{Ca}$  than their host rocks, interorb matrices, and orbicule cores (Fig. 3 A and B and SI Appendix, Tables S5 and S6), suggestive of especially fast growth rates.

The small bulk rock subsamples drilled across 2 orbicules (core-to-rim,  $n = 28$ ; SI Appendix) are mineralogically more

complex, with  $\delta^{44}\text{Ca}$  variations across the layers (ranging from 0.0 to  $-0.5\text{\textperthousand}$ ; SI Appendix, Table S5) generally anticorrelated with Ca concentrations and positively correlated with Fe and Mg concentrations (Fig. 3C). The observations suggest that  $\delta^{44}\text{Ca}$  is mostly controlled by mineral abundances in the different layers, with greater abundances of mafic minerals being associated with higher  $\delta^{44}\text{Ca}$ . By measuring major cation concentrations in the different subsamples of the largest orbicule (Fig. 3D), however, we identify 2 regions where changes in  $\delta^{44}\text{Ca}$  (ranging from  $-0.2$  to  $-0.5\text{\textperthousand}$ ) are positively correlated with Ca and are not accompanied by changes in Fe and Mg. This combination suggests kinetic control on  $\delta^{44}\text{Ca}$  for these layers (Fig. 3 C and D and SI Appendix, Fig. S3).

Diffusive kinetic Ca isotope effects during mantle metasomatism and high-temperature (high-T) metamorphism have also been described in previous studies (22, 30). In the former case, the authors observed relatively large negative  $\Delta^{44}\text{Ca}_{\text{oxp-cpx}}$  in Fe-rich peridotites and used analytical diffusion models to arrive at estimates for the product of diffusivity and time [ $Dt$  (30)] during metasomatic Ca diffusion into pyroxene grains. In the latter case, the authors used a numerical model for diffusion in heterogeneous media combining spatial, chemical, and Ca isotopic constraints, along with independent timing constraints for metamorphism, to estimate effective Ca diffusivities and isotopic diffusivity ratios ( $D_{44}/D_{40}$ ) during high-T metamorphism of the lower crust (22). Although both of these models are phenomenologically different from the model at hand (due to the different geologic processes), they highlight the utility of combining  $\delta^{44}\text{Ca}$  constraints with diffusion models in order to better understand the nature and duration of disequilibrium processes in Earth's interior.

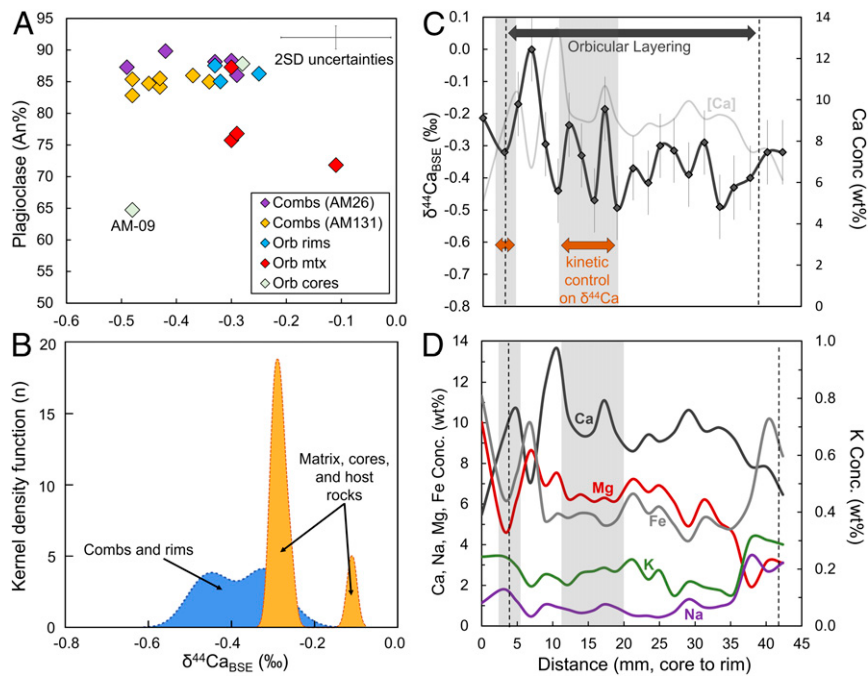


**Fig. 3.** Ca isotope and chemical compositions in (A and B) plagioclase separates from orbicules, comb layers, and related samples from Fisher Lake ( $n = 23$ ), and (C and D) bulk rock subsamples across a dioritic orbicule (Emerald Bay,  $n = 22$ ). We exclude orb-core sample AM-09 from B on the basis that it represents a different primary lithology (olivine norite, instead of hornblende gabbro; *SI Appendix*). Dashed lines represent the extent of orbicular layering. In A and C, Ca concentrations are from isotope dilution TIMS; in D, cation concentrations are from ICP-OES; see *SI Appendix* for details. Ca isotopic measurements are reported relative to bulk silicate Earth (+0.96‰ relative to SRM915a). Error bars represent long-term 2 SD uncertainties on  $\delta^{44}\text{Ca}$  ( $\pm 0.1\%$ ).

### Growth-Rate Estimates

We focus our modeling on plagioclase, because it is a commonly occurring mineral that crystallizes in a range of magma compositions (e.g., ref. 31) and because the equilibrium melt-mineral fractionation can be assumed to be approximately zero. Using our  $\Delta^{44}\text{Ca}$  measurements and conservative estimates for the previously discussed parameters (*SI Appendix*, Fig. S6), we estimate  $R/D$  for our samples (Fig. 4) assuming  $\Delta^{44}\text{Ca}_{\text{plag-melt}} = 0$  at equilibrium. Growth rates are calculated using a Ca diffusivity of  $10 \text{ cm}^2/\text{y}$  ( $\sim 10^{-11} \text{ m}^2/\text{s}$ ). For the plagioclase separates from orbicules and comb layers, we assume that variations in  $\delta^{44}\text{Ca}_{\text{plag}}$  are the results of variations in crystal growth rates. For bulk rock subsamples from kinetically controlled orbicule layers (Fig. 3 C and D), we assume that the host rock chemical and isotopic compositions are the same as the original magma (*SI Appendix*).

Growth-rate estimates for our various samples are shown in Fig. 4. Two of our plagioclase phenocryst separates cannot be isotopically distinguished from their matrix materials, thus indicating growth rates of less than  $\sim 4$  and  $\sim 1 \text{ cm/y}$ , respectively (different due to different Ca distribution coefficients in MLV-6R and MLV-6). Phenocryst samples from Deadman Creek Dome (93MLV-49) and the Mount Lassen 1915 rhyodacite eruption, however, show resolvable  $\Delta^{44}\text{Ca}_{\text{plag-mtx}}$  differences suggesting minimum growth rates of  $\sim 0.7$  and  $\sim 7 \text{ cm/y}$  (Fig. 4B). These rates are  $\sim 2$  and  $\sim 20$  times faster, respectively, than the rates commonly assumed for phenocryst growth in decompressing magmas (e.g., refs. 8 and 32). These growth-rate values are high but not unreasonable, given the high crystallization rates ( $\sim 10 \text{ cm/y}$ ) observed in supercooled experimental magmas (33), upon which previous timescale estimates in subvolcanic orbicules and comb layers were based (17), and the observation that experimental feldspar spherulite crystals can grow at rates as high as  $\sim 30 \text{ cm/y}$  (34).

The larger kinetic effects in our orbicule and comb layer samples suggest faster growth rates than in the volcanic phenocrysts (Fig. 4), with speeds up to  $\sim 25 \text{ cm/y}$  (minimum values of

$\sim 6 \text{ cm/y}$  to  $\sim 15 \text{ cm/y}$ ; Fig. 4C). These fast growth rates compare favorably to previous estimates for orbicules and suggest that the parameters we had to estimate for our models are reasonable (*SI Appendix*). Attainment of the predicted steady-state solutions (Eq. 1) depends on boundary layer thickness relative to crystal size (*SI Appendix*), with small boundary layers favoring quicker development of steady-state growth conditions (20). If steady state were not reached in our measured samples, this would lead to incompletely expressed fractionations and suggests that our growth rates would serve as minimum estimates. Similarly, our orbicule and comb layer plagioclase separates may also contain late-stage interstitial plagioclase grown closer to equilibrium, so it is likely that the disequilibrium  $\Delta^{44}\text{Ca}$  signatures we measure are minimum values for rapidly grown plagioclase populations within a sample. This averaging also applies for our volcanic phenocryst separates, where various populations of plagioclase phenocrysts (up to 3 per sample, physically mixed together by our mineral separations; estimated abundances in *SI Appendix*, Table S7) may have grown at different rates.

### Timescales for Crystallization and Magmatic Recharge

CSD analyses are commonly used to estimate nucleation rates and crystallization timescales in volcanic samples (e.g., refs. 8 and 32), and also allow for identification of separate phenocryst populations within a sample (*SI Appendix*). Crystal growth rates, however, are required as necessary inputs to calculate both timescales and nucleation rates, and are typically poorly constrained [varying by over 5 orders of magnitude in natural samples (7)]. Using well-established techniques for CSD analyses (*SI Appendix*, Figs. S8 and S9) and combining the results with our growth-rate estimates based on Ca isotope analyses, we can better constrain crystallization timescales in volcanic samples.

Based on CSD slopes (*SI Appendix*, Fig. S8), large plagioclase phenocrysts in 02DLA-1 and 93MLV-49 (minimum growth rates of 7 and  $0.7 \text{ cm/y}$ , respectively) are likely to have grown in  $\sim 5$  and

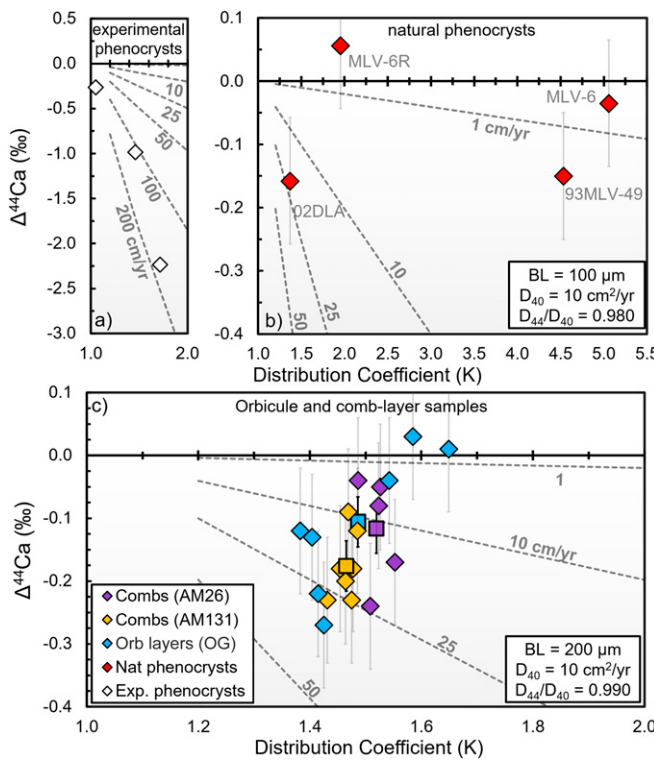


**Fig. 4.**  $\Delta^{44}\text{Ca}$  vs. Ca distribution coefficients for analyzed plagioclase separates from (A and B) experimental (Exp.;  $n = 3$ ) and natural (Nat.) phenocryst samples ( $n = 4$ ) along with (C) separates from orbicule and comb layer samples (Emerald Bay and Fisher Lake,  $n = 19$ ) with dashed contours representing predictions for various crystal growth rates, based on Eq. 1. In A and B,  $\Delta^{44}\text{Ca}$  represents  $\delta^{44}\text{Ca}$  differences between plagioclase and glass/matrix, and we assume  $D_{44}/D_{40} = 0.980$ , in accordance with ref. 36 (SI Appendix, Fig. S6), and BL of  $100 \mu\text{m}$  [suggested as maximum values in dynamic systems (38); SI Appendix]. In C,  $D_{44}/D_{40} = 0.990$  and  $\Delta^{44}\text{Ca}$  represents kinetic effects based on differences for plagioclase  $\delta^{44}\text{Ca}$  (Fisher Lake) or non-mineralogical  $\delta^{44}\text{Ca}$  differences from interorbicule matrix (Emerald Bay; SI Appendix). We use larger BL sizes of  $200 \mu\text{m}$  to account for larger crystal sizes in the orbs and comb layers (SI Appendix). Rate estimates are directly proportional to BL, such that 1/2 a given BL leads to double the required growth rate. Average values and 2 SE for Fisher Lake samples (AM26, AM131) and kinetic layers in OG sample (Emerald Bay) are represented by colored squares ( $n = 3$ ) with bold error bars in C. Results using higher  $D_{44}/D_{40}$  are shown in SI Appendix, Fig. S7 for comparison.

~30 d, respectively (SI Appendix, Fig. S10 and Table S8). Assuming the same growth rates as for the large phenocrysts, small plagioclase microlites in these 2 samples (SI Appendix, Fig. S9) are estimated to have grown in as little as ~2 h and ~1 d, respectively (SI Appendix, Fig. S10). Although the crystal growth rates of individual plagioclase populations cannot be estimated from our mineral separates, which represent average values for the phenocryst populations in a sample, previous work on Mount Lassen samples indicates that plagioclase microlites are likely to have grown much faster than larger phenocrysts (35). This conclusion suggests that the plagioclase microlites in our samples are likely to have larger disequilibrium Ca isotopic signatures than the phenocrysts and are thus important targets for future studies.

For samples where phenocryst  $\delta^{44}\text{Ca}$  could not be distinguished from equilibrium values, including mafic clinopyroxene and amphibole phenocrysts, we present CSD-based growth timescales assuming a common value for crystal growth rates in decompressing magmas (0.3 cm/y) (e.g., refs. 8, 32, and 35), and find that these represent timescales ranging from ~1 d to ~330 d (SI Appendix, Fig. S10 and Table S8), which are generally shorter

than currently available diffusion-based estimates for magmas with similarly silicic compositions (7). Plagioclase microlites have the shortest growth timescales, ranging from ~1 d to 3 d. Amphibole phenocrysts in Black Butte yield a timescale of ~200 d, while clinopyroxene in approximate Ca isotopic equilibrium with melt (in Mount Lassen, 02DLA) suggests timescales of ~40 d to ~90 d for crystallization (SI Appendix, Table S8), in agreement with previous CSD work on plagioclase from this locality (35). Distinct populations of plagioclase phenocrysts in Mono Crater (MLV-6) yield ~330 and ~60 d for the large and medium phenocrysts, respectively, which is consistent with the shortest timescales previously determined for similar systems (7).

The orbicule and comb layer samples (with minimum growth rates ranging from 6 cm/y to 15 cm/y) cannot be used for CSD analyses, due to their unique textures, but, based on the sizes of the largest crystals (up to ~1 cm; SI Appendix, Table S8), the applicable growth timescales are likely to be ~20 d to ~50 d. Performing a similarly simple estimate based on the maximum crystal sizes in our natural phenocryst samples leads to timescales 2 to 6 times longer than when using our CSD constraints (SI Appendix, Table S8), which may suggest that these timescales are upper limits. Comparing our Ca isotope-based estimates to results from other methods (Fig. 5), we find general agreement with diffusion profile estimates in mafic samples, but significantly shorter timescales for silicic systems.

## Discussion

The timescales deduced from our growth-rate estimates for mafic orbicules and comb layers are in general agreement with diffusion profile estimates for mafic volcanic phenocrysts (7).

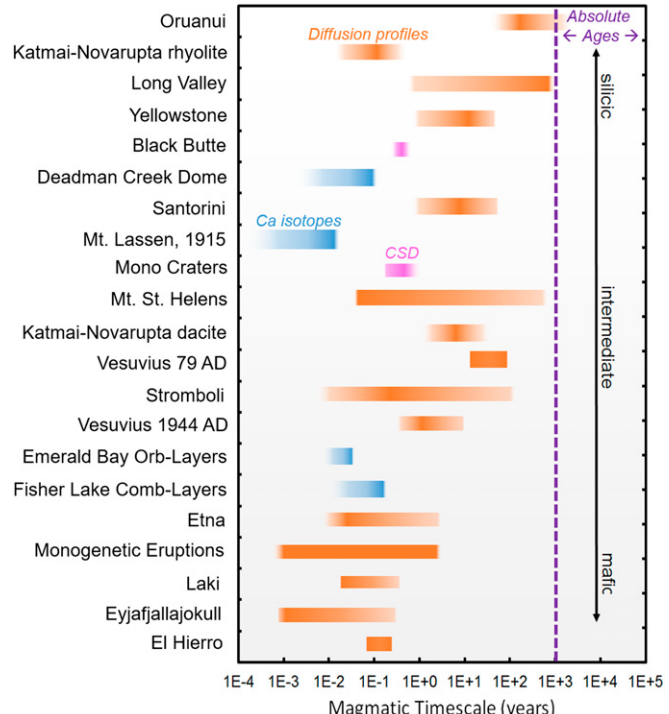


**Fig. 5.** Magmatic timescales from absolute crystal ages (purple) and diffusion profiles (orange), based on ref. 7 and references therein, compared to our results based on kinetic Ca isotope effects (blue) and CSD-only estimates (pink). Phenocryst growth timescale estimates (Mount Lassen, 1915 and Deadman Creek Dome) are from a combination of Ca isotope growth-rate estimates and CSD analyses. Orbicule and comb layer estimates (Emerald Bay and Fisher Lake) are based on maximum crystal sizes (SI Appendix). Ca isotopes indicate similarly short timescales for both mafic and silicic compositions.

These samples provide constraints directly linked to growth in subvolcanic conduits during magmatic recharge episodes (17, 18). The observation that timescales for orbicule and comb layer growth are similar to those deduced from volcanic phenocrysts supports the idea that diffusion profiles in mafic crystals faithfully record the duration of magmatic recharge events.

Our timescale estimates in silicic systems, however, while similar to those inferred for mafic systems, are much shorter than previous estimates (Fig. 5). Although our study is principally investigating the use of Ca isotopes as a growth-rate proxy in volcanic systems, and does not provide a comprehensive overview of all magmatic compositions, the short durations inferred for phenocryst growth in silicic systems challenge the accepted model of increasing timescales with increasing SiO<sub>2</sub> content (7). Our results suggest that mafic and silicic systems have similar lengths of time between magmatic rejuvenation and volcanic eruption, and that the previously observed relationship might be due to inaccurate estimates for crystal growth rates and/or analytical biases.

The Ca isotope method has an advantage in that it can be used in all magma compositions that contain plagioclase. Nevertheless, the effects are typically subtle, and further work should evaluate 1) different plagioclase phenocryst populations within a sample, 2) experimental phenocryst growth in varying magma compositions, and 3) boundary layer variations and compositions in natural systems. Experimental studies have found that Ca isotope fractionation during diffusion in magmas is also sensitive to the strength and direction of diffusion for other chemical species (e.g., refs. 36 and 37). These studies, however, have only investigated a limited number of anhydrous magmatic compositions and conditions, and more experimental work would be needed in order to incorporate multicomponent diffusion effects into our growth-rate models.

## Conclusions

We show that disequilibrium Ca isotope effects are produced during growth of experimental and natural phenocrysts, orbicular rocks, and comb layers, in accordance with previous theoretical predictions (20). Relatively large  $\Delta^{44}\text{Ca}$  effects (>2‰) are possible in H<sub>2</sub>O-poor experimental melts with fast cooling rates, but the size of the effects decreases with increasing H<sub>2</sub>O abundances, due to increasing Ca diffusivity in the magma. We

show that crystal growth rates during formation of natural plagioclase comb layers and orbicule layers can exceed 6 cm/y to 15 cm/y, implying timescales of 1 mo to 2 mo for the formation of individual layers and for the duration of magmatic recharge and crystallization events in mafic systems. Plagioclase phenocrysts from the 1915 Mount Lassen rhyodacite eruption and the ~650-y-old Deadman Creek Dome eruption have disequilibrium  $\Delta^{44}\text{Ca}_{\text{plag-matrix}}$  compositions consistent with minimum growth rates of ~7 and 0.7 cm/y, respectively. In combination with CSD analyses, these growth rates imply timescales of ~5 d and ~1 mo for phenocryst crystallization, which are significantly shorter than estimates from diffusion profiles in other silicic magmas (7), but are approximately the same as our timescale estimates for mafic systems. The timescales deduced from our Ca isotope approach add to a growing body of evidence suggesting that volcanic systems can undergo rapid reactivation and eruption triggered by the injection of fresh magma into subvolcanic reservoirs, even if they are stored at cold temperatures for extended time periods (e.g., refs. 2–4, 7–9, and 11–16). We show that the Ca isotope method can be applied across a wide variety of magma compositions, and hence has the potential to further our understanding of eruptive processes over the full range of magmatic systems.

## Materials and Methods

TIMS at the University of California, Berkeley, was used to measure stable Ca isotope compositions in a large suite of volcanic and subvolcanic phenocrystic, orbicular, and comb layer rocks, including experimental and natural plagioclase phenocrysts and matrix, mafic phenocrysts, and small whole-rock subsamples. CSD analyses were performed on perpendicular cuts of large hand samples and X-ray maps of thin sections. Chemical analyses were performed by X-ray fluorescence (XRF) and optical emission spectroscopy (ICP-OES). Model parameters for our crystal growth estimates, CSD methods/results, sample descriptions, and analytical details can be found in *SI Appendix*.

**ACKNOWLEDGMENTS.** We thank N. Botto, S. Mulcahey, W. Yang, T. Teague, and S. T. Brown for their technical expertise, and C. T. Lee for sharing an orbicule sample and micro-XRF data. This research was primarily supported by US National Science Foundation Grant EAR100500 (to D.J.D.). M.A.A. acknowledges Natural Sciences and Engineering Research Council of Canada postgraduate funding that aided in supporting this work. T.M. acknowledges graduate funding from NSF Grant EAR1615203.

- National Academies of Sciences, Engineering, and Medicine, *Volcanic Eruptions and Their Repose, Unrest, Precursors, and Timing* (National Academies Press, Washington, DC, 2017).
- A. Burgisser, G. W. Bergantz, A rapid mechanism to remobilize and homogenize highly crystalline magma bodies. *Nature* **471**, 212–215 (2011).
- S. E. Gelman, F. J. Gutiérrez, O. Bachmann, On the longevity of large upper crustal silicic magma reservoirs. *Geology* **41**, 759–762 (2013).
- C. Huber, O. Bachmann, J. Dufek, Crystal-poor versus crystal-rich ignimbrites: A competition between stirring and reactivation. *Geology* **40**, 115–118 (2012).
- R. S. J. Sparks *et al.*, Formation and dynamics of magma reservoirs. *Philos. Trans. A Math. Phys. Eng. Sci.* **377**, 20180019 (2019).
- K. Cooper, Crystal ages and timescales of magma reservoir processes. *Geochim. Cosmochim. Acta* **70**, A111 (2006).
- K. M. Cooper, Time scales and temperatures of crystal storage in magma reservoirs: Implications for magma reservoir dynamics. *Philos. Trans. A Math. Phys. Eng. Sci.* **377**, 20180009 (2019).
- K. M. Cooper, A. J. R. Kent, Rapid remobilization of magmatic crystals kept in cold storage. *Nature* **506**, 480–483 (2014).
- A. E. Rubin *et al.*, Rapid cooling and cold storage in a silicic magma reservoir recorded in individual crystals. *Science* **356**, 1154–1156 (2017).
- A. K. Schmitt, Uranium series accessory crystal dating of magmatic processes. *Annu. Rev. Earth Planet. Sci.* **39**, 321–349 (2011).
- T. H. Druitt, F. Costa, E. Deloule, M. Dungan, B. Scaillet, Decadal to monthly timescales of magma transfer and reservoir growth at a caldera volcano. *Nature* **482**, 77–80 (2012).
- O. Bachmann, G. W. Bergantz, Rhyolites and their source mushes across tectonic settings. *J. Petrol.* **49**, 2277–2285 (2008).
- O. Bachmann, C. F. Miller, S. L. de Silva, The volcanic-plutonic connection as a stage for understanding crustal magmatism. *J. Volcanol. Geotherm. Res.* **167**, 1–23 (2007).
- J. W. Davis, D. S. Coleman, J. T. Gracely, R. Gaschnig, M. Stearns, Magma accumulation rates and thermal histories of plutons of the Sierra Nevada batholith, CA. *Contrib. Mineral. Petroil.* **163**, 449–465 (2012).
- L. Karlstrom, M. L. Rudolph, M. Manga, Caldera size modulated by the yield stress within a crystal-rich magma reservoir. *Nat. Geosci.* **5**, 402–405 (2012).
- C. Annen, From plutons to magma chambers: Thermal constraints on the accumulation of eruptible silicic magma in the upper crust. *Earth Planet. Sci. Lett.* **284**, 409–416 (2009).
- A. McCarthy, O. Müntener, Comb layering monitors decompressing and fractionating hydrous mafic magmas in subvolcanic plumbing systems (Fisher Lake, Sierra Nevada, USA). *J. Geophys. Res. Solid Earth* **121**, 8595–8621 (2016).
- A. McCarthy, O. Müntener, Mineral growth in melt conduits as a mechanism for igneous layering in shallow arc plutons: Mineral chemistry of Fisher Lake orbicules and comb layers (Sierra Nevada, USA). *Contrib. Mineral. Petroil.* **172**, 1–32 (2017).
- M. H. Ort, Orbicular volcanic rocks of Cerro Panizos: Their origin and implications for orb formation. *Geol. Soc. Am. Bull.* **104**, 1048–1058 (1992).
- E. B. Watson, T. Müller, Non-equilibrium isotopic and elemental fractionation during diffusion-controlled crystal growth under static and dynamic conditions. *Chem. Geol.* **267**, 111–124 (2009).
- B. A. Tripoli, B. Cordonnier, A. Zappone, P. Ulmer, Effects of crystallization and bubble nucleation on the seismic properties of magmas. *Geochem. Geophys. Geosyst.* **17**, 602–615 (2016).
- M. A. Antonelli *et al.*, Kinetic and equilibrium Ca isotope effects in high-T rocks and minerals. *Earth Planet. Sci. Lett.* **517**, 71–82 (2019).
- F. Huang, C. Zhou, W. Wang, J. Kang, Z. Wu, First-principles calculations of equilibrium Ca isotope fractionation: Implications for oldhamite formation and evolution of lunar magma ocean. *Earth Planet. Sci. Lett.* **510**, 153–160 (2019).
- H. Zhang *et al.*, No measurable calcium isotopic fractionation during crystallization of Kilauea Iki lava lake. *Geochem. Geophys. Geosyst.* **19**, 3128–3139 (2018).
- M. E. Holycross, E. B. Watson, F. M. Richter, J. Villeneuve, Diffusive fractionation of Li isotopes in wet, silicic melts. *Geochem. Perspect. Lett.* **6**, 39–42 (2018).
- D. J. DePaolo, G. J. Wasserburg, Sm-Nd age of the Stillwater complex and the mantle evolution curve for neodymium. *Geochim. Cosmochim. Acta* **43**, 999–1008 (1979).
- W. Wang *et al.*, Effect of Ca content on equilibrium Ca isotope fractionation between orthopyroxene and clinopyroxene. *Geochim. Cosmochim. Acta* **219**, 44–56 (2017).
- C. Feng, T. Qin, S. Huang, Z. Wu, F. Huang, First-principles investigations of equilibrium calcium isotope fractionation between clinopyroxene and Ca-doped orthopyroxene. *Geochim. Cosmochim. Acta* **143**, 132–142 (2014).

29. A. McCarthy, O. Müntener, A. S. Bouvier, L. Baumgartner, Melt extraction zones in shallow arc plutons: Insights from fisher lake orbicules (Sierra Nevada, Western USA). *J. Petrol.* **57**, 2011–2052 (2016).
30. X. Zhao *et al.*, Coupled extremely light Ca and Fe isotopes in peridotites. *Geochim. Cosmochim. Acta* **208**, 368–380 (2017).
31. J. Blundy, K. Cashman, M. Humphreys, Magma heating by decompression-driven crystallization beneath andesite volcanoes. *Nature* **443**, 76–80 (2006).
32. C. R. Brugger, J. E. Hammer, Crystal size distribution analysis of plagioclase in experimentally decompressed hydrous rhyodacite magma. *Earth Planet. Sci. Lett.* **300**, 246–254 (2010).
33. T. Shea, J. E. Hammer, Kinetics of cooling- and decompression-induced crystallization in hydrous mafic-intermediate magmas. *J. Volcanol. Geotherm. Res.* **260**, 127–145 (2013).
34. F. Arzilli *et al.*, Near-liquidus growth of feldspar spherulites in trachytic melts: 3D morphologies and implications in crystallization mechanisms. *Lithos* **216–217**, 93–105 (2015).
35. M. J. Salisbury, W. A. Bohrson, M. A. Clyne, F. C. Ramos, P. Hoskin, Multiple plagioclase crystal populations identified by crystal size distribution and in situ chemical data: Implications for timescales of magma chamber processes associated with the 1915 eruption of Lassen Peak, CA. *J. Petrol.* **49**, 1755–1780 (2008).
36. J. M. Watkins, D. J. DePaolo, E. B. Watson, Kinetic fractionation of non-traditional stable isotopes by diffusion and crystal growth reactions. *Rev. Mineral. Geochem.* **82**, 85–125 (2017).
37. J. M. Watkins, Y. Liang, F. Richter, F. J. Ryerson, D. J. DePaolo, Diffusion of multi-isotopic chemical species in molten silicates. *Geochim. Cosmochim. Acta* **139**, 313–326 (2014).
38. F. Lu, A. T. Anderson, A. M. Davis, Diffusional gradients at the crystal/melt interface and their effect on the compositions of melt inclusions. *J. Geol.* **103**, 591–597 (1995).